

Article

A Comparison of the Mechanisms and Activation Barriers for Ammonia Synthesis on Metal Nitrides (Ta_3N_5 , Mn_6N_5 , $\text{Fe}_3\text{Mo}_3\text{N}$, $\text{Co}_3\text{Mo}_3\text{N}$)

Constantinos D. Zeinalipour-Yazdi 

Faculty of Computing, Mathematics, Engineering and Natural Sciences, Northeastern University London, London E1W 1LP, UK; zeinalip@gmail.com or constantinos.zeinalipour@nulondon.ac.uk

Abstract: In this study we perform a comparison of the reaction mechanism and the activation barrier for the rate-determining step in various metal nitrides (Ta_3N_5 , Mn_6N_5 , $\text{Fe}_3\text{Mo}_3\text{N}$, $\text{Co}_3\text{Mo}_3\text{N}$) for the ammonia synthesis reaction. The reactions are explained with simplified schematics and the energy profiles for the various reaction mechanisms are given in order to screen the catalytic activity of the catalysts for the ammonia synthesis reaction. We find that the catalytic activity ranks in the following order: $\text{Co}_3\text{Mo}_3\text{N} > \text{Fe}_3\text{Mo}_3\text{N} > \text{Ta}_3\text{N}_5 > \text{Mn}_6\text{N}_5$. We also find that the reaction mechanism proceeds either by a Langmuir–Hinshelwood and an Eley–Rideal/Mars–van Krevelen mechanism. This is an overview of about 10 years of computational research conducted to provide an overview of the progress established in this field of study.

Keywords: ammonia synthesis; mechanism; cobalt molybdenum nitride; tantalum nitride; manganese nitride; iron molybdenum nitride; DFT



Citation: Zeinalipour-Yazdi, C.D. A Comparison of the Mechanisms and Activation Barriers for Ammonia Synthesis on Metal Nitrides (Ta_3N_5 , Mn_6N_5 , $\text{Fe}_3\text{Mo}_3\text{N}$, $\text{Co}_3\text{Mo}_3\text{N}$). *Crystals* **2024**, *14*, 392. <https://doi.org/10.3390/cryst14050392>

Academic Editor: Nikolaus Korber

Received: 22 March 2024

Revised: 19 April 2024

Accepted: 21 April 2024

Published: 23 April 2024



Copyright: © 2024 by the author. Licensee MDPI, Basel, Switzerland. This article is an open access article distributed under the terms and conditions of the Creative Commons Attribution (CC BY) license (<https://creativecommons.org/licenses/by/4.0/>).

1. Introduction

The ammonia synthesis reaction is one of the milestones of chemistry, spanning a history of over 100 years of industrial development [1–3]. Currently, the catalyst most used industrially is a potassium oxide-promoted iron catalyst which operates at high temperatures (450–550 °C) and pressures (100–200 atm) and undergoes a Langmuir–Hinshelwood (L–H) mechanism [4,5]. The mechanism of ammonia synthesis on Fe(211) and Fe_3 clusters was elucidated theoretically very recently [6,7]. Since ammonia is produced globally in vast amounts, currently represents about 50% of the product used by humans, and requires about 2% of the global energy use, it is desirable to find catalysts to synthesize it in a more sustainable way. Therefore, metal nitrides that can operate at lower temperatures and pressures have been suggested as alternatives to the iron catalyst. There is also a ruthenium-supported graphite catalyst that is used in small-scale industrial plants for ammonia synthesis that operates at more moderate temperatures (200–300 °C) [8]. In this catalyst, an $-\text{N}_2\text{H}$ intermediate was found to be important and it was discovered that the reaction mechanism is associative [9].

When we started investigating the mechanism of ammonia synthesis on cobalt molybdenum nitride, only a handful of previous studies had computationally studied this and assumed that the surface intermediates are $-\text{N}$ and $-\text{H}$ [10] and that an L–H mechanism operates [11]. Other kinetic studies have applied Brønsted–Evans–Polanyi (BEP) relationships that correlated the dissociation barrier to the adsorption energy of N_2 [10,12]. We have set out to understand the mechanism of ammonia synthesis on cobalt molybdenum nitride ($\text{Co}_3\text{Mo}_3\text{N}$), which is known to be a more active catalyst for ammonia synthesis than the iron catalysts, especially when doped with caesium [10,11,13,14]. For $\text{Co}_3\text{Mo}_3\text{N}$ metal support, interactions with crystalline MgO support have been found to be beneficial for the activity of this catalyst [15]. The optimum feedstock composition was investigated using ammonia synthesis rate measurements [16]. For this catalyst, we found that there are

two competing mechanism in which ammonia is synthesised in: (1) via the conventional Langmuir–Hinshelwood (L–H) mechanism, and (2) via an Eley–Rideal/Mars–van Krevelen (E–R) mechanism [17,18]. Following this study, we modelled the reaction mechanism for ammonia synthesis on tantalum nitride (Ta_3N_5) [19], manganese nitride (Mn_6N_5) [20], and iron molybdenum nitride ($\text{Fe}_3\text{Mo}_3\text{N}$) [21], but generally found lower activity than the $\text{Co}_3\text{Mo}_3\text{N}$ catalyst. There have also been studies by other groups concerning the mechanism of the ammonia synthesis reaction on metal nitrides. For example, Younes Abghoui and Egill Skúlason, who investigated Zr, Nb, Cr, and V mononitrides [22,23] for the electrochemical reduction in ammonia and in a two-step solar-energy driven ammonia synthesis on metal nitrides, found nitrogen vacancies to be important catalytic centres [24,25]. Furthermore, in the study of the electrochemical synthesis of ammonia on group III–VII transition metal nitrides, NbN was found to be suitable [26]. The $\text{Co}_3\text{Mo}_3\text{N}$ catalyst, when doped with Cs, was found to produce H_2 from ammonia via a decomposition pathway [27]. Furthermore, spatially resolved $\text{Co}_3\text{Mo}_3\text{N}$ particles on SBA-15 were found to have enhanced catalytic activity by Said Laassiri and co-workers [28]. Recently, enhanced nitrogen activation was observed in the electrochemical synthesis of ammonia over a composite $\text{Co}_3\text{Mo}_3\text{N}$ and $\text{La}_{0.6}\text{Sr}_{0.4}\text{Co}_{0.2}\text{Fe}_{0.8}\text{O}_3$ perovskite cathode [29].

For the first time, the different mechanisms that are happening on chemically related materials are studied with respect to ammonia synthesis. The computational process of elucidating a reaction mechanism is tedious and is attempted for one material/catalyst at the time. However, in this study, by combining the results of a series of papers on related materials (i.e., metal nitrides), we show that we can rank them in terms of activity on the basis of the activation barrier of the rate-determining step. This study should inspire other computational chemists to try ranking materials based on catalytic activity of the potential energy diagram for the reaction.

2. Materials and Methods

All calculations were completed with the plane-wave code VASP 4 and VASP 5 [30,31]. The unit cell of each metal nitride was optimised by changing the lattice vectors and atomic positions, and then that unit cell was used to generate the slab. All DFT calculations were Γ -point [32] spin-polarised calculations within the generalized gradient approximation (GGA) using the revised Perdew–Burke–Ernzerhof (revPBE) exchange–correlation (XC) functional [33], with the projector augmented-wave (PAW) method [34,35] used to represent core states. The force threshold on the geometry optimisations was $0.02 \text{ eV } \text{Å}^{-1}$ and the convergence criterion for electronic relaxation was 10^{-4} eV . The plane-wave cutoff was set to 800 eV and the k-point convergence was achieved for the $4 \times 4 \times 1$ Monkhorst-Pack grid for the Ta_3N_5 . The plane-wave cutoff was set to 600 eV for the Mn_6N_5 system with a k-point grid of $2 \times 2 \times 1$. The cutoff energy for the $\text{Co}_3\text{Mo}_3\text{N}$ and $\text{Fe}_3\text{Mo}_3\text{N}$ system was set to 650 eV using a $4 \times 4 \times 1$ k-point grid.

Grimme’s dispersion corrections were included via the zero-damping DFT-D3 correction method [36], in which the following dispersion energy correction is added to the Kohn–Sham energies,

$$E_{disp} = -\frac{1}{2} \sum_{i=1}^N \sum_{j=1}^N \left(s_6 \frac{C_{6,ij}}{r_{ij}^6} + s_8 \frac{C_{8,ij}}{r_{ij}^8} \right), \quad (1)$$

where $C_{6,ij}$ and $C_{8,ij}$ denote the averaged (isotropic) 6th and 8th order dispersion coefficients for atom pair ij and r_{ij} is the internuclear distance between atoms i and j , respectively. s_6 and s_8 are the functional-dependent scaling factors.

The Nudged Elastic Band (NEB) method was used to calculate activation barriers [37] using five images to map out the barrier.

3. Results and Discussion

3.1. Cobalt Molybdenum Nitride ($\text{Co}_3\text{Mo}_3\text{N}$)

The Eley–Rideal/Mars–van Krevelen mechanism is shown in Figure 1a. The active site for the catalytic cycle is a nitrogen vacancy on the molybdenum nitride framework. Molecular nitrogen chemisorbs at the N-vacancies in an end-on configuration and then molecular hydrogen chemisorbs dissociatively onto the molecular nitrogen, forming a diazene intermediate. Following this, another molecular hydrogen from the gas phase physisorbs molecularly at an adjacent molybdenum nitride centre, as shown in C'. The molecular physisorbed hydrogen then reacts with the diazene intermediate, forming a hydrazine intermediate and an atomically chemisorbed H as shown in D'. The hydrazine intermediate dissociates, forming the first stoichiometric ammonia in a low barrier process, leaving behind on the surface of the catalyst a nitrate and atomic hydrogen, as shown in E'. The atomic hydrogen then moves to the nitride forming $-\text{NH}$. Subsequently, another molecular hydrogen physisorbs at the molybdenum nitride framework where it reacts with the $-\text{NH}$ forming $-\text{NH}_2$, as shown in H'. Following this, the atomic hydrogen from the molybdenum nitride framework reacts with $-\text{NH}_2$ forming $-\text{NH}_3$ as shown in I'. This ammonia molecule desorbs from a catalyst in a high barrier process, indicating that the catalyst surface may be covered with ammonia after a few catalytic cycles.

The Langmuir–Hinshelwood mechanism is shown in Figure 1b. The active site for this mechanism can be found at the interface of the cobalt clusters and the molybdenum nitride framework. In this mechanism, molecular nitrogen adsorbs side-on at the active site and is significantly activated (i.e., 21%), as shown in A. The activated nitrogen undergoes dissociation and forms two bridged N-species, as shown in B. Then, H_2 chemisorbs dissociatively on the cobalt cluster, as shown in C. H then reacts with the bridged-N species, forming a $>\text{N-H}$ intermediate, as shown in D, which moves to a hollow position at the Mo_3 site. Another H reacts with N-H forming $>\text{NH}_2$ at a bridge site of the cobalt cluster, as shown in E. In F, another H_2 adsorbs dissociatively on the cobalt cluster. In G, the 3f-bound-N to the Mo_3 hollow moves due to surface diffusion to the adjacent Co- Mo_2 hollow, while displacing NH_3 chemisorbs on the Co_8 cluster. In H, 3f-bound-N at Co- Mo_2 hollow moves to the adjacent bridge position at Co_8 , reacting with H and forming an $>\text{NH}$ intermediate. In J, H_2 adsorbs dissociatively on the cobalt cluster, forming in K a $>\text{NH}_2$ intermediate. In L, a third H atom reacts with $>\text{NH}_2$, forming $>\text{NH}_3$, which then desorbs from the active site of the L–H mechanism, as shown in M.

In Figure 2, we compare the Langmuir–Hinshelwood (L–H) with the Eley–Rideal/Mars–van Krevelen (E–R) mechanism and we can observe that all barriers for the hydrogenation steps in the L–H mechanism are larger than the E–R mechanism. This gives a clear indication that the E–R mechanism of cobalt molybdenum nitride is a kinetically faster mechanism and will be the main mechanism for ammonia synthesis over $\text{Co}_3\text{Mo}_3\text{N}$.

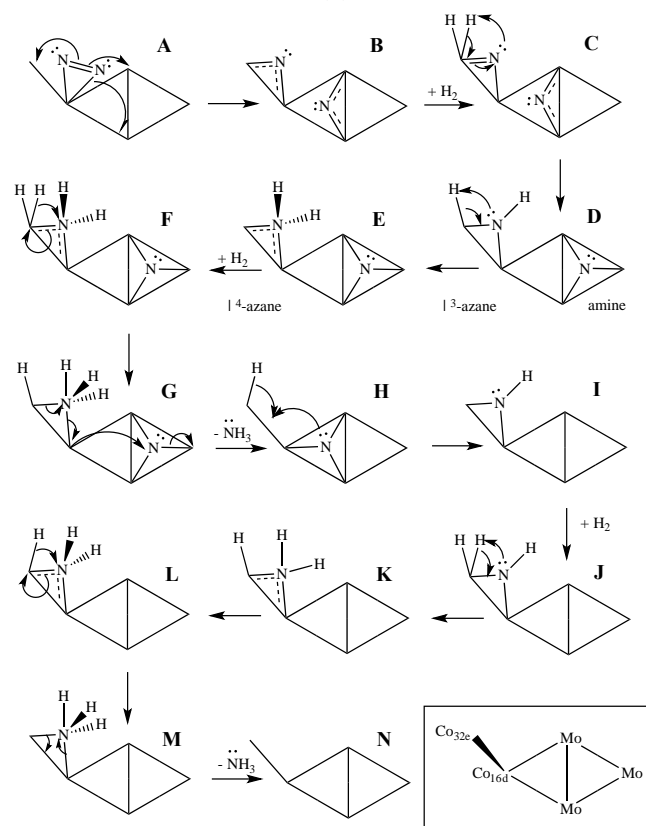
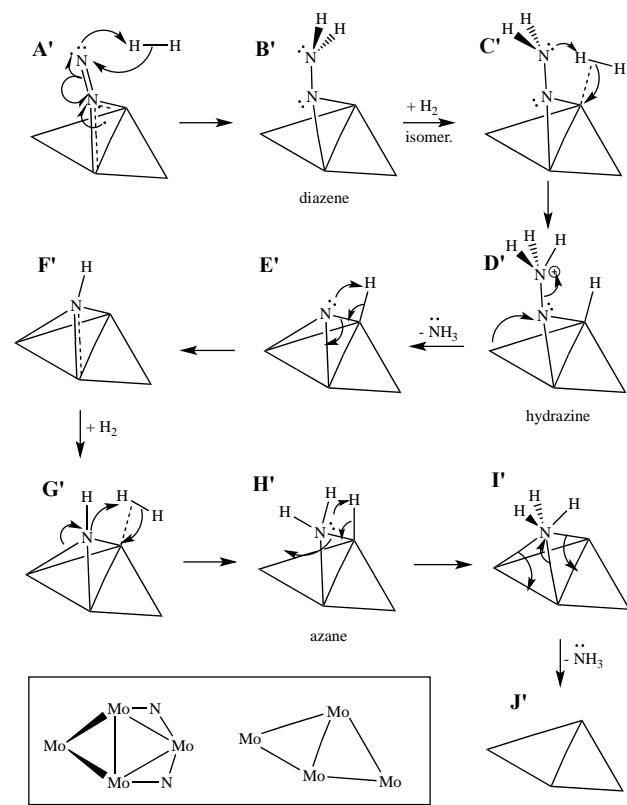


Figure 1. (a) Eley–Rideal/Mars–van Krevelen (associative) Mechanism (b) Langmuir–Hinshelwood (dissociative) mechanism for ammonia synthesis on $\text{Co}_3\text{Mo}_3\text{N}$ reproduced from Ref. [18] with permission.

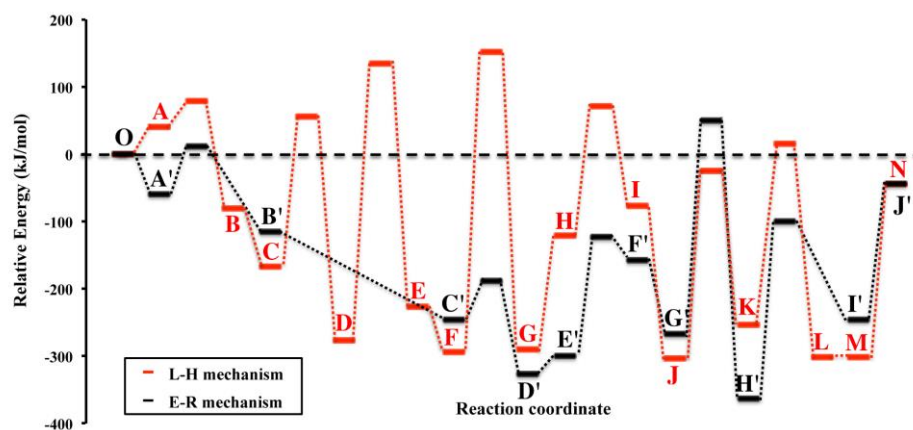


Figure 2. Relative energy diagram of Langmuir–Hinshelwood (red) and Eley–Rideal/Mars–van Krevelen (black) mechanism for ammonia synthesis on $\text{Co}_3\text{Mo}_3\text{N}$ surfaces. Energies in reference with the empty surface with one nitrogen vacancy, $3\text{H}_2(\text{g})$, and $\text{N}_2(\text{g})$, reproduced from Ref. [18] with permission.

3.2. Tantalum Nitride (Ta_3N_5)

The mechanism of ammonia synthesis on tantalum nitride starts again with a nitrogen vacancy, as shown in O of Figure 3. Molecular nitrogen chemisorbs at this N-vacancy in a side-on configuration. Subsequently, molecular hydrogen chemisorbs in a side-on configuration at an adjacent tantalum centre, as shown in B. Another molecular hydrogen from the gas phase chemisorbs at the other tantalum centre of the catalytic site, as shown in C. The molecularly chemisorbed hydrogen then dissociates and reacts with the chemisorbed nitrogen, forming initially NN-H, as shown in D. This step has a barrier of 50 kJ/mol, which is a relatively moderate barrier for hydrogenation. In a subsequent step, another molecular hydrogen dissociates, reacting with NN-H and forming H-NN-H, as shown in E. The H-NN-H species then moves to the adjacent tantalum site, forming in the process an ammonia molecule, as shown in F. This intermediate generates the first stoichiometric ammonia in a rather high barrier step ($\text{F} \rightarrow \text{G}$). In the following step, molecular hydrogen chemisorbs on the tantalum atom that does not have any preadsorbed hydrogen, as shown in H. This molecular hydrogen then dissociates, forming a $-\text{NH}$ species, as shown in I. Subsequently, the atomic chemisorbed hydrogen from the nearby tantalum sites hydrogenates the $-\text{NH}$, forming initially $>\text{NH}_2$, as shown in J. Then the $>\text{NH}_2$ reacts with $-\text{H}$, forming ammonia that is adsorbed to the tantalum atom, as shown in K. The ammonia desorbs from the catalytic site in a high barrier process, indicating that the catalytic site may be poisoned by adsorbed ammonia. The details of all the activation barriers are shown in Figure 4 and it generally appears that the tantalum nitride catalyst is less reactive than the $\text{Co}_3\text{Mo}_3\text{N}$ catalyst.

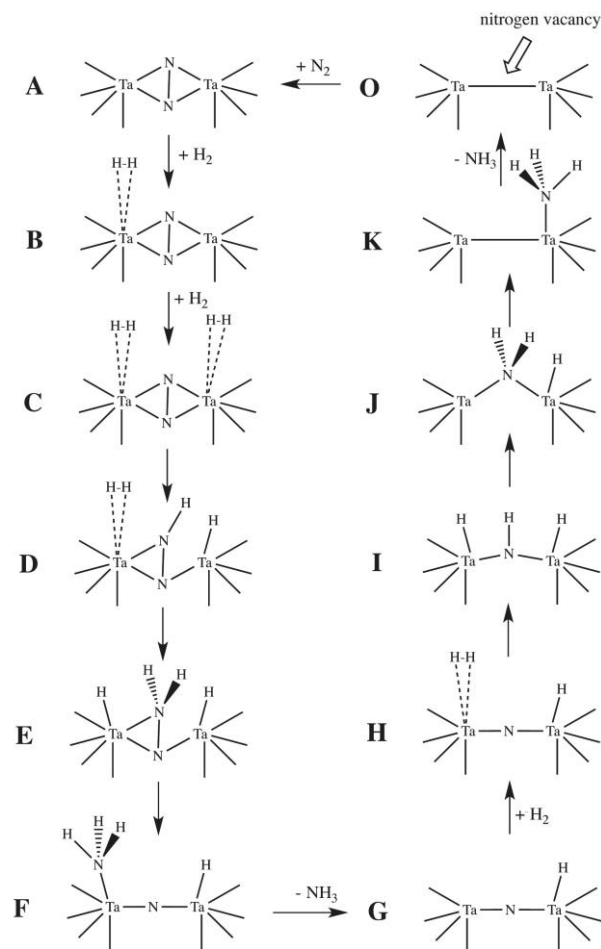


Figure 3. Ammonia synthesis at nitrogen vacancies of the Ta₃N₅-(100) surface. The mechanism initiates at O with the adsorption of dinitrogen to a nitrogen vacancy. Figure reproduced with permission from Ref. [38].

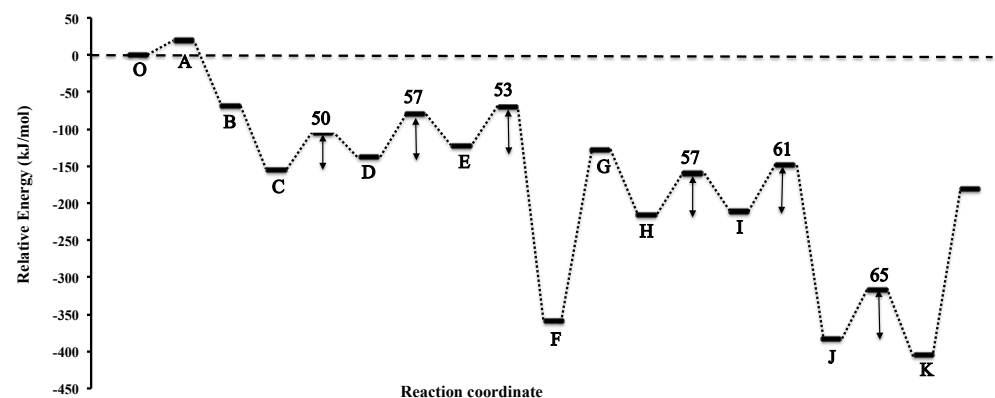


Figure 4. Potential energy diagram of ammonia synthesis reaction mechanism on (100)-Ta₃N₅ reproduced with permission from Ref. [38].

3.3. Manganese Nitride (Mn₆N₅)

The mechanism of ammonia synthesis of manganese nitride starts again with nitrogen vacancies at the surface of the (111) surface. Molecular nitrogen chemisorbs in an end-on configuration at these nitrogen vacancies and on the Mn atoms, as shown in Figure 5 in B and C. Molecular hydrogen that physisorbs on these N₂ sites then reacts with them in a high barrier process, forming -NNH₂. The same happens for the N₂ adsorbed onto the

Mn atoms, which also forms $-\text{NNH}_2$. Subsequently, molecular hydrogen interacts with two $-\text{NNH}_2$ species on the surface, simultaneously forming two ammonia molecules that are adsorbed on nitrogens of the manganese nitride framework. When these ammonia molecules desorb, which happens in two consecutive steps in a relatively low barrier process, all nitrogen vacancy sites on the surface of the catalyst are occupied. At this point, molecular hydrogen chemisorbs on the nitrogen of the manganese nitride framework, and in a moderate barrier process forms $>\text{NH}_2$, as shown in M. This happens also for another nitrogen on the (111) surface of Mn_6N_5 , forming a second $>\text{NH}_2$ species, as shown in O. After this, molecular hydrogen interacts with two $>\text{NH}_2$ species, forming two ammonia molecules that are chemisorbed on the Mn atoms, as shown in P. These ammonia molecules desorb in a relatively high-energy process, leaving the surface exposed to nitrogen vacancy sites that act as catalytic centres for the upcoming catalytic cycles. The differences of this mechanism from the one occurring on $\text{Co}_3\text{Mo}_3\text{N}$ is that molecular hydrogen reacts in an Eley–Rideal type mechanism during the formation of ammonia, which, however, is found to be a high-barrier process on this catalyst. Therefore, this catalyst has the lowest activity for ammonia synthesis compared to the other metal nitrides in this study. The potential energy diagram for this reaction mechanism is depicted in Figure 6 and shows that the surface of the catalyst is poisoned by $-\text{NNH}_2$ species and that increasing the concentration or partial pressure of hydrogen in the feedstream may have a positive effect on the kinetics of this reaction on Mn_6N_5 .

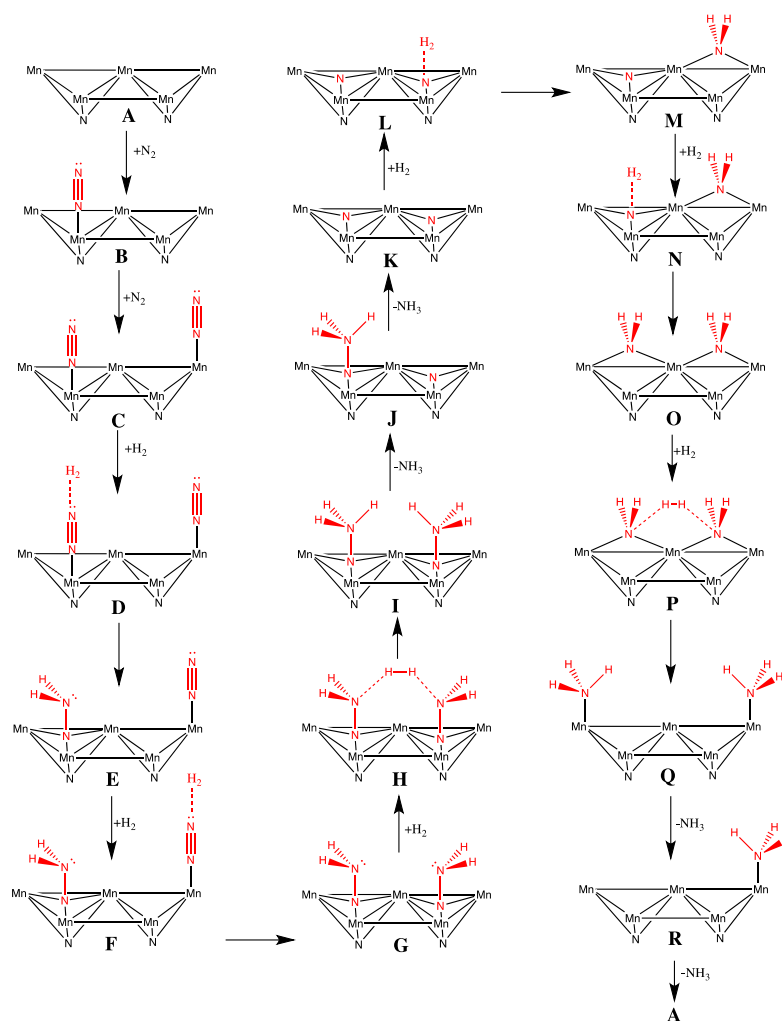


Figure 5. Reaction mechanism for ammonia synthesis via an Eley–Rideal mechanism on $\theta\text{-Mn}_6\text{N}_5$ -(111) reproduced with permission from Ref. [20]. Catalyst shown in black and intermediates shown in red.

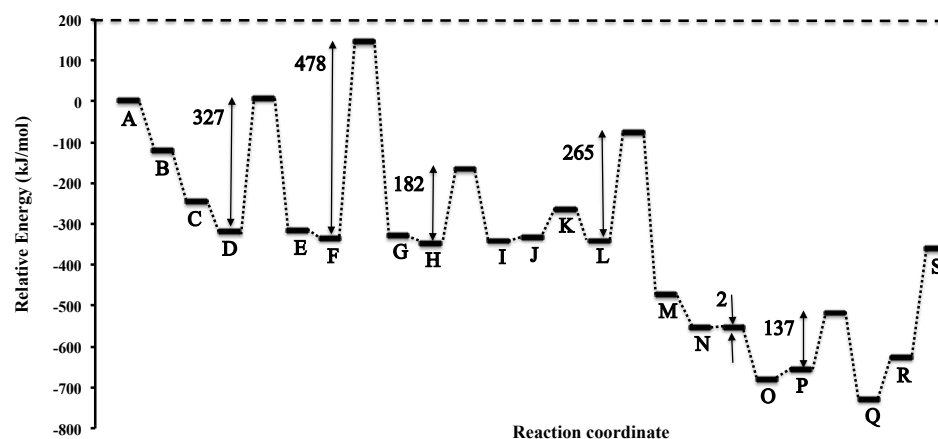


Figure 6. Potential energy diagram of ammonia synthesis reaction via Eley–Rideal mechanism on θ - Mn_6N_5 -(111) slab without surface nitrogen vacancy reproduced with permission from Ref. [20].

3.4. Iron Molybdenum Nitride ($\text{Fe}_3\text{Mo}_3\text{N}$)

The E–R mechanism of ammonia synthesis of iron molybdenum nitride is the same as the mechanism for cobalt molybdenum nitride. From the barriers of the reaction mechanism, as shown in Figure 7, it becomes clear that the $\text{Fe}_3\text{Mo}_3\text{N}$ catalyst is less reactive than the $\text{Co}_3\text{Mo}_3\text{N}$ catalyst for ammonia synthesis. In particular, all hydrogenation steps are high-barrier processes. However, the desorption of ammonia from the catalyst requires less energy compared to the hydrogenation steps. The barriers for the reaction pathway indicate that $\text{Fe}_3\text{Mo}_3\text{N}$ is less reactive than $\text{Co}_3\text{Mo}_3\text{N}$ for ammonia synthesis but more reactive than Ta_3N_5 and Mn_6N_5 .

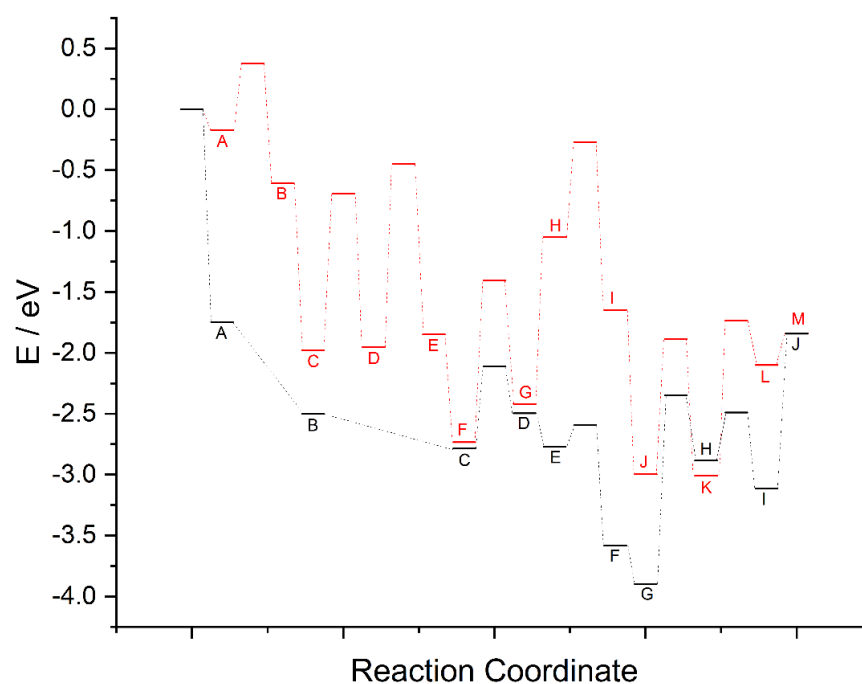


Figure 7. Potential energy diagram of ammonia synthesis reaction via Eley–Rideal/Mars–van Krevelen mechanism on $\text{Co}_3\text{Mo}_3\text{N}$ (black) and $\text{Fe}_3\text{Mo}_3\text{N}$ (red) reproduced with permission from Ref. [21].

The future of ammonia synthesis research using computational tools relies on the use of aspects coming from kinetics to rank catalytic materials based on their activity. This so far has been a tedious process which requires exact knowledge of the reaction mechanism and calculation of all the barriers for the reaction. Currently, we are not aware of another

study where different reaction mechanisms are considered for ammonia synthesis to rank catalytic materials.

Future directions of this research would be to study the mechanism of ammonia synthesis on other metal nitrides and attempt to find a mechanism that has a lower barrier for the RDS of cobalt molybdenum nitride. This would direct the way of computational screening of catalysts that at the moment is in its infancy. Also, finding softwares that can map out the mechanism of reactions using automated methods and methods that invoke machine learning is a possible direction.

There are definitely limitations and challenges for computational-only studies of reaction mechanisms. The first limitation is that DFT calculations have an accuracy of 1–2 kJ/mol, which can make a significant difference when we start talking about the rate and the activity of different materials. Also, in some cases, as has been shown for $\text{Co}_3\text{Mo}_3\text{N}$, the catalytic materials undergo degradation, which will definitely affect the mechanism [39]. Currently, taking into account various phases of the catalyst that are not the ones derived from X-ray crystallography is challenging and should be considered with care in future studies using computational tools.

The industrial use of catalyst for ammonia production is a long and slow process. For example, the Ru/Graphite catalyst was first studied computationally before it was used for small-scale ammonia synthesis production. Therefore, such ranking of catalytic materials is very advantageous as it can save time, resources, and funding from experimental efforts to improve these catalysts. It is without any doubt that the computational ranking of catalytic materials for ammonia synthesis will accelerate the discovery of new catalysts that are more active than the existing catalysts. We are therefore in the era that new experiments will be informed by computational studies of this kind more frequently.

4. Conclusions

We screened the activity of various metal nitrides using DFT calculations for the ammonia synthesis reaction. We found that the metal nitrides invoke nitrogen vacancies as catalytic sites for the ammonia synthesis reaction, but they proceed with different mechanisms. $\text{Co}_3\text{Mo}_3\text{N}$ and $\text{Fe}_3\text{Mo}_3\text{N}$ undergo an Eley–Rideal/Mars–van Krevelen mechanism that is associative. Ta_3N_5 undergoes a Langmuir–Hinshelwood mechanism for ammonia synthesis, which again happens at nitrogen vacancies. Mn_6N_5 undergoes an Eley–Rideal mechanism for ammonia synthesis, but the kinetics are not great because of the high barrier for the hydrogenation step of surface nitrogen. Following analysis of the activation energy barriers for the various mechanisms on metal nitrides, we find the following trend for the activity of these metal nitrides for ammonia synthesis: $\text{Co}_3\text{Mo}_3\text{N} > \text{Fe}_3\text{Mo}_3\text{N} > \text{Ta}_3\text{N}_5 > \text{Mn}_6\text{N}_5$.

Funding: This research was funded by EPSRC, grant number EP/L026317/1, EP/L02537X/1, via our membership in the UK's HEC Materials Chemistry Consortium, which is funded by EPSRC (EP/L000202/1). This work used the ARCHER UK National Supercomputing Service (<http://www.archer.ac.uk>).

Data Availability Statement: The original contributions presented in the study are included in the article, further inquiries can be directed to the corresponding author.

Conflicts of Interest: The author declares no conflicts of interest.

References

1. Ertl, G.; Knözinger, H.; Weitkamp, J. *Handbook of Heterogeneous Catalysis*; VCH: Weinheim, Germany, 1997; Volume 2.
2. Ertl, G.; Lee, S.B.; Weiss, M. Kinetics of nitrogen adsorption on Fe(111). *Surf. Sci.* **1982**, *114*, 515–526. [[CrossRef](#)]
3. Erisman, J.W.; Sutton, M.A.; Galloway, J.; Klimont, Z.; Winiwarter, W. How a century of ammonia synthesis changed the world. *Nat. Geosci.* **2008**, *1*, 636. [[CrossRef](#)]
4. Ertl, G. Surface Science and Catalysis—Studies on the Mechanism of Ammonia Synthesis: The P. H. Emmett Award Address. *Catal. Rev.* **1980**, *21*, 201–223. [[CrossRef](#)]
5. Bowker, M. Modelling of ammonia synthesis kinetics. *Catal. Today* **1992**, *12*, 153–163. [[CrossRef](#)]
6. Fuller, J.; Fortunelli, A.; Goddard, W.A., III; An, Q. Reaction mechanism and kinetics for ammonia synthesis on the Fe(211) reconstructed surface. *Phys. Chem. Chem. Phys.* **2019**, *21*, 11444–11454. [[CrossRef](#)]

7. Liu, J.-C.; Ma, X.-L.; Li, Y.; Wang, Y.-G.; Xiao, H.; Li, J. Heterogeneous Fe₃ single-cluster catalyst for ammonia synthesis via an associative mechanism. *Nat. Commun.* **2018**, *9*, 1610. [[CrossRef](#)]
8. Saadatjou, N.; Jafari, A.; Sahebdehfar, S. Ruthenium Nanocatalysts for Ammonia Synthesis: A Review. *Chem. Eng. Commun.* **2015**, *202*, 420–448. [[CrossRef](#)]
9. Garden, A.L.; Skúlason, E. The Mechanism of Industrial Ammonia Synthesis Revisited: Calculations of the Role of the Associative Mechanism. *J. Phys. Chem. C* **2015**, *119*, 26554–26559. [[CrossRef](#)]
10. Boisen, A.; Dahl, S.; Jacobsen, C.J.H. Promotion of Binary Nitride Catalysts: Isothermal N₂ Adsorption, Microkinetic Model, and Catalytic Ammonia Synthesis Activity. *J. Catal.* **2002**, *208*, 180–186. [[CrossRef](#)]
11. Jacobsen, C.J.H.; Dahl, S.; Clausen, B.S.; Bahn, S.; Logadóttir, A.; Nørskov, J.K. Catalyst Design by Interpolation in the Periodic Table: Bimetallic Ammonia Synthesis Catalysts. *J. Am. Chem. Soc.* **2001**, *123*, 8404–8405. [[CrossRef](#)]
12. Nørskov, J.; Bligaard, T.; Logadóttir, A.; Bahn, S.; Hansen, L.; Bollinger, M.; Benggaard, H.; Hammer, B.; Slijivančanin, Z.; Mavrikakis, M.; et al. Universality in Heterogeneous Catalysis. *J. Catal.* **2002**, *209*, 275–278. [[CrossRef](#)]
13. Kojima, R.; Aika, K.-I. Cobalt Molybdenum Bimetallic Nitride Catalysts for Ammonia Synthesis. *Chem. Lett.* **2000**, *5*, 514–515. [[CrossRef](#)]
14. Kojima, R.; Aika, K.-I. Cobalt molybdenum bimetallic nitride catalysts for ammonia synthesis: Part 1. Preparation and characterization. *Appl. Catal. A Gen.* **2001**, *215*, 149–160. [[CrossRef](#)]
15. Rai, R.K.; Maligal-Ganesh, R.; Maksoud, W.A.; Kim, S.-J.; Vaishnav, Y.; Yavuz, C.T.; Kobayashi, Y. Enhancing Ammonia Synthesis on Co₃Mo₃N via Metal Support Interactions on a Single-crystalline MgO Support. *ChemCatChem* **2024**, e202301579. [[CrossRef](#)]
16. Aslan, M.Y.; Hargreaves, J.S.J.; Uner, D. The effect of H₂:N₂ ratio on the NH₃ synthesis rate and on process economics over the Co₃Mo₃N catalyst. *Faraday Discuss.* **2021**, *229*, 475–488. [[CrossRef](#)] [[PubMed](#)]
17. Zeinalipour-Yazdi, C.D.; Hargreaves, J.S.J.; Catlow, C.R.A. Nitrogen Activation in a Mars–van Krevelen Mechanism for Ammonia Synthesis on Co₃Mo₃N. *J. Phys. Chem. C* **2015**, *119*, 28368–28376. [[CrossRef](#)]
18. Zeinalipour-Yazdi, C.D.; Hargreaves, J.S.J.; Catlow, C.R.A. Low-T Mechanisms of Ammonia Synthesis on Co₃Mo₃N. *J. Phys. Chem. C* **2018**, *122*, 6078–6082. [[CrossRef](#)]
19. Zeinalipour-Yazdi, C.D.; Hargreaves, J.S.J.; Laassiri, S.; Catlow, C.R.A. DFT-D3 study of H₂ and N₂ chemisorption over cobalt promoted Ta₃N₅-(100), (010) and (001) surfaces. *Phys. Chem. Chem. Phys.* **2017**, *19*, 11968–11974. [[CrossRef](#)]
20. Zeinalipour-Yazdi, C.D. On the possibility of an Eley–Rideal mechanism for ammonia synthesis on Mn₆N_{5+x} (x = 1)-(111) surfaces. *Phys. Chem. Chem. Phys.* **2018**, *20*, 18729–18736. [[CrossRef](#)] [[PubMed](#)]
21. Higham, M.D.; Zeinalipour-Yazdi, C.D.; Hargreaves, J.S.J.; Catlow, C.R.A. Mechanism of ammonia synthesis on Fe₃Mo₃N. *Faraday Discuss.* **2023**, *243*, 77–96. [[CrossRef](#)] [[PubMed](#)]
22. Abghoui, Y.; Garden, A.L.; Hlynsson, V.F.; Björgvinsdóttir, S.; Olafsdóttir, H.; Skúlason, E. Enabling electrochemical reduction of nitrogen to ammonia at ambient conditions through rational catalyst design. *Phys. Chem. Chem. Phys.* **2015**, *17*, 4909–4918. [[CrossRef](#)] [[PubMed](#)]
23. Abghoui, Y.; Garden, A.; Howat, J.; Vegge, T.; Skúlason, E. Electroreduction of N₂ to Ammonia at Ambient Conditions on Mononitrides of Zr, Nb, Cr, and V: A DFT Guide for Experiments. *ACS Catal.* **2016**, *6*, 635–646. [[CrossRef](#)]
24. Michalsky, R.; Pfromm, P.; Steinfeld, A. Rational Design of Metal Nitride Redox Materials for Solar-Driven Ammonia Synthesis. *Interface Focus* **2015**, *5*, 20140084. [[CrossRef](#)] [[PubMed](#)]
25. Michalsky, R.; Avram, A.; Peterson, B.; Pfromm, P.; Peterson, A. Chemical Looping of Metal Nitride Catalysts: Low-Pressure Ammonia Synthesis for Energy Storage. *Chem. Sci.* **2015**, *6*, 3965–3974. [[CrossRef](#)] [[PubMed](#)]
26. Abghoui, Y.; Skúlason, E. Electrochemical synthesis of ammonia via Mars-van Krevelen mechanism on the (111) facets of group III–VII transition metal mononitrides. *Catal. Today* **2017**, *286*, 78–84. [[CrossRef](#)]
27. Srifa, A.; Okura, K.; Okanishi, T.; Muroyama, H.; Matsui, T.; Eguchi, K. Hydrogen production by ammonia decomposition over Cs-modified Co₃Mo₃N catalysts. *Appl. Catal. B Environ.* **2017**, *218*, 1–8. [[CrossRef](#)]
28. Sfeir, A.; Teles, C.A.; Ciotonea, C.; Reddy, G.N.M.; Marinova, M.; Dhainaut, J.; Löfberg, A.; Dacquin, J.-P.; Royer, S.; Laassiri, S. Enhancing ammonia catalytic production over spatially confined cobalt molybdenum nitride nanoparticles in SBA-15. *Appl. Catal. B Environ.* **2023**, *325*, 122319. [[CrossRef](#)]
29. Ferree, M.; Gunduz, S.; Kim, J.; LaRosa, R.; Khalifa, Y.; Co, A.C.; Ozkan, U.S. Enhanced N₂ Activation on a Composite Co₃Mo₃N Nitride and La_{0.6}Sr_{0.4}Co_{0.2}Fe_{0.8}O₃ Perovskite Cathode for High-Temperature Electrochemical Ammonia Synthesis. *ACS Sustain. Chem. Eng.* **2023**, *11*, 5007–5013. [[CrossRef](#)]
30. Kresse, G.; Furthmüller, J. Efficient iterative schemes for ab initio total-energy calculations using a plane-wave basis set. *Phys. Rev. B* **1996**, *54*, 11169–11186. [[CrossRef](#)] [[PubMed](#)]
31. Kresse, G.; Hafner, J. Ab initio Molecular Dynamics for Liquid Metals. *Phys. Rev. B* **1993**, *47*, 558. [[CrossRef](#)] [[PubMed](#)]
32. Monkhorst, H.; Pack, J. Special points for Brillouin-zone integrations. *Phys. Rev. B* **1976**, *13*, 5188. [[CrossRef](#)]
33. Perdew, J.; Burke, K.; Ernzerhof, M. Generalized gradient approximation made simple. *Phys. Rev. Lett.* **1996**, *77*, 3865. [[CrossRef](#)] [[PubMed](#)]
34. Blöchl, P. Projector augmented-wave method. *Phys. Rev. B* **1994**, *50*, 17953. [[CrossRef](#)] [[PubMed](#)]
35. Kresse, G.; Joubert, D. From ultrasoft pseudopotentials to the projector augmented-wave method. *Phys. Rev. B* **1999**, *59*, 1758–1775. [[CrossRef](#)]

36. Grimme, S.; Antony, J.; Ehrlich, S.; Krieg, H.A. Consistent and Accurate ab initio Parametrization of Density Functional Dispersion Correction (DFT-D) for the 94 Elements H-Pu. *J. Chem. Phys.* **2010**, *132*, 154104. [[CrossRef](#)] [[PubMed](#)]
37. Mills, G.; Jónsson, H.; Schenter, G. Reversible Work Transition State Theory: Application to Dissociative Adsorption of Hydrogen. *Surf. Sci.* **1995**, *324*, 305–337. [[CrossRef](#)]
38. Zeinalipour-Yazdi, C.D. Mechanistic aspects of ammonia synthesis on Ta₃N₅ surfaces in the presence of intrinsic nitrogen vacancies. *Phys. Chem. Chem. Phys.* **2021**, *23*, 6959–6963. [[CrossRef](#)] [[PubMed](#)]
39. Hunter, S.M.; McKay, D.; Smith, R.I.; Hargreaves, J.S.J.; Gregory, D.H. Topotactic Nitrogen Transfer: Structural Transformation in Cobalt Molybdenum Nitrides. *Chem. Mater.* **2010**, *22*, 2898–2907. [[CrossRef](#)]

Disclaimer/Publisher’s Note: The statements, opinions and data contained in all publications are solely those of the individual author(s) and contributor(s) and not of MDPI and/or the editor(s). MDPI and/or the editor(s) disclaim responsibility for any injury to people or property resulting from any ideas, methods, instructions or products referred to in the content.